

An efficient Moving Morphable Component (MMC)-based approach for multi-resolution topology optimization

Chang Liu¹, Yichao Zhu¹, Zhi Sun¹, Dingding Li¹, Zongliang Du^{1,2*},
Weisheng Zhang¹, Xu Guo^{1*}

*¹State Key Laboratory of Structural Analysis for Industrial Equipment,
Department of Engineering Mechanics,
International Research Center for Computational Mechanics,
Dalian University of Technology, Dalian, 116023, P.R. China*

*²Structural Engineering Department,
University of California, San Diego, San Diego, CA 92093, United States of America*

Abstract

In the present work, a highly efficient Moving Morphable Component (MMC) based approach for multi-resolution topology optimization is proposed. In this approach, high-resolution optimization results can be obtained with much less number of degrees of freedoms (DOFs) and design variables since the topology optimization model and the finite element analysis model are totally decoupled in the MMC-based problem formulation. This is achieved by introducing super-elements for structural response analysis and adopting a domain decomposition strategy to preserve the topological complexity of optimized structures. Both two-and three-dimensional numerical results demonstrate that substantial computational efforts can be saved for large-scale topology optimization problems with use of the proposed approach.

Keywords: Moving Morphable Component (MMC), Multi-Resolution Topology Optimization, Large-Scale Problems, Computational Efficiency, Topological Complexity.

*Corresponding authors. E-mail: zldu@mail.dlut.edu.cn (Zongliang Du), guoxu@dlut.edu.cn (Xu Guo)

1. Introduction

Structural topology optimization, which aims at distributing a certain amount of available materials within a prescribed design domain appropriately in order to achieve optimized structural performances, has been extended to a wide range of physical disciplines such as acoustics, electromagnetics, and optics since the pioneering work of Bendsoe and Kikuchi (1988). So far, classical topology optimization methods have already been implemented in commercial softwares (e.g., Altair-OptiStruct (HyperWorks, 2013) and Abaqus (Simulia, 2011)) to solve practical problems. However, due to the large computational efforts associated with the solution of topology optimization problems where systems of (sometimes nonlinear) partial differential equations must be solved iteratively to find the structural responses and sensitivity information, topology optimization methods are not easy to be applied to large-scale problems especially when high-resolution designs containing structural features with small length scales are sought for.

In traditional implicit topology optimization methods (e.g., the Solid Isotropic Material with Penalization (SIMP) method, the level set method (LSM)), the finite element analysis (FEA) model and the topology description model are strongly coupled. This means that the density of the FE mesh determines not only the accuracy of FEA, but also the resolution of the obtained optimized solutions. Under this circumstance, very fine FE meshes must be employed if high-resolution designs containing structural features with very small length scales are sought for. This will inevitably lead to large-scale and time consuming computational tasks especially for three-dimensional (3D) topology optimization problems. For example, if a cubic design domain is discretized into $100 \times 100 \times 100$ elements along three coordinate directions, a FE model with 3 million degrees of freedoms (DOFs) as well as a nonlinear optimization problem with 1 million design variables must be dealt with at every step of the iterative solution process. Furthermore, if we intend to double the resolution to retain more tiny structural features in the optimized design, the corresponding numbers of the DOFs and design variables would increase to 24 million and 8 million, respectively! Recently, with use of a supercomputer with 8000 processors, Aage et al. (2017) found the optimal reinforcement of a full aircraft wing with 1.1 billion voxels for FE discretization via SIMP method in several days. This, however, is almost an impossible task for ordinary computers.

To promote the practical application of topology optimization, many attempts have been made to enhance the solution efficiency of large-scale optimization problems. One direct approach is to use high performance computing resources and parallelize the solution process. To be specific, early research works mainly focused on how to obtain structural responses rapidly with use of parallelization techniques (Borrvall and Petersson (2011), Kim et al. (2004), Vemaganti and Lawrence (2005), Evgrafov et al. (2007), Mahdavi et al. (2006), Aage et al. (2007)). Moreover, in order to reduce the computational time associated with the solution of large-scale nonlinear optimization problems with a huge number of design variables, Aage and Lazarov (2013) also parallelized the well-known MMA optimizer successfully. Although these achievements greatly enhanced the capability of solving large-scale topology optimization problems, the corresponding computational complexity is not reduced essentially. Besides resorting to high performance computing (HPC) techniques, some researchers have also made attempts to enhance the efficiency of FEA by employing some special solution schemes or reducing the total number of DOFs in FEA models directly. For example, Wang et al. (2007) proposed to recycle parts of the search space in a Krylov subspace solver to reduce the number of iterations for solving the equilibrium equations, and significant saving of computational effort is observed especially when the changes of design variables between two consecutive optimization steps are small enough. Amir et al. (2009a) proposed a solution procedure in which exact FEA is performed only at certain stages of iterations while approximate reanalysis is used elsewhere; in Amir et al. (2009b), an alternative stopping criterion for a Preconditioned Conjugate Gradient (PCG) iterative solver was adopted so that fewer iterations are required for obtaining a converged solution. Amir and Sigmund (2010) also proposed an approximate approach to solve the nested analysis equations, and it was reported that the computational cost can be reduced by one order of magnitude. It should be pointed out, however, that the above techniques are generally suitable for dealing with some specific classes of problems and need careful elaborations for extensive applications.

Form the aspect of simplifying the FEA model, adaptive mesh refinement techniques (Kim et al. (2003), Stainko (2005), Guest and Smith Genut (2010)) and model reduction method (Yoon (2010)) have been introduced in the implicit SIMP-based solution framework. More recently, Nguyen et al. (2009) proposed a multi-resolution formulation for minimum compliance designs based on a coarse FE mesh for structural response

analysis and a finer mesh for density field discretization. Later on, this approach had been further extended to involve an adaptive mesh refinement scheme (Nguyen et al. 2012). Although the number of DOFs in FEA models can be greatly reduced, the number of design variables is still very large in the aforementioned approaches, which, as will be shown later, also requires a large amount of computational time (corresponding to the solution of large-scale nonlinear/non-convex optimization problems) when large-scale multi-resolution topology optimization problems are considered. Besides, in order to eliminate numerical instabilities such as the checkerboard phenomenon, additional strategies such as the density filtering technique with a prescribed length scale (usually greater than the size of the coarse mesh) have to be introduced. Such treatments, however, would inevitably lead to boundary diffusion effect and the loss of structural details with small feature sizes. As a result, although the resolution for the density field is enhanced, the filtered structural boundary is still blurry, and most important of all, the complexity of structural topology of optimized structures cannot be preserved. In addition, due to the implicit nature of geometry descriptions, post-processing is always required to transfer the optimized designs obtained by implicit topology optimization approaches to computer aided design/engineering (CAD/CAE) systems. This issue to some extent as well restricted the application of the aforementioned multi-resolution topology optimization approach to large-scale problems which often lead to heavier and more complex post-processing works.

To overcome the aforementioned challenging issues for solving large-scale multi-resolution optimization problems, in the present paper, the Moving Morphable Components (MMC)-based topology optimization approach is extended to the multi-resolution framework. The MMC-based topology optimization method was first initialized by Guo et al. (2014), where a number of structural components with explicit geometry descriptions are adopted as basic building blocks of optimization (see in Fig. 1 for reference). Therefore, optimized designs can be determined by optimizing the explicit geometry parameters characterizing the sizes, shapes and layouts of the introduced components. Compared with traditional topology optimization approaches, in the MMC method, topology optimization can be achieved in an explicit and geometrical way. It has been shown that this new solution framework not only can reduce the number of design variables substantially but also has the merit of easily controlling the structural geometry features such as minimum length scale (Zhang et al. (2016a)), overhang angle (Guo et al.

(2017)) and the connectivity of a structure (Deng and Chen (2016)) in an explicit and flexible way. Actually, recent years witnessed a growing interest on developing topology optimization methods based on explicit geometry/topology descriptions (Guo et al. (2016), Zhang et al. (2016b, 2016c, 2017a, 2017b, 2017c, 2018a, 2018b), Liu et al. (2017), Xue et al. (2017), Norato et al. (2015), Zhang et al. (2016, 2017d, 2018), Zhang and Norato (2017), Zhang et al. (2017e, 2017f), Hoang and Jang (2017), Hou et al. (2017), Takaloozadeh and Yoon (2017) and Sun et al. (2018)).

As pointed in Guo et al. (2014) and Zhang et al. (2016c), one of the distinctive features of the MMC-based topology optimization framework is that the corresponding FEA model and the topology description model are *totally decoupled*. In previous implementation of the MMC-based approaches (Guo et al. (2014, 2016, 2017), Zhang et al. (2016a, 2016b, 2016c, 2017b, 2017c, 2018a), Liu et al. (2017), Xue et al. (2017)), since the same mesh is used for both the interpolation of displacement field and the projection of the explicit geometry, the unique decoupling advantage of the MMC method has not been fully utilized. In the present work, we propose to adopt two sets of meshes with different resolutions for FEA and topology description, respectively, to establish a highly efficient multi-resolution MMC-based solution framework for structural topology optimization. Actually, as will be shown in the forthcoming sections, compared with traditional methods, under the proposed MMC-based multi-resolution framework, the computation time for FEA can be reduced by one order of magnitude, and more importantly high-resolution designs can be obtained with a smaller number of design variables.

The rest of the paper is organized as follows. In Section 2, the problem formulation under the MMC-based solution framework is presented. Then the strategy of obtaining high-resolution designs efficiently using MMCs as basic building blocks of optimization is described in Section 3. Afterwards, some techniques, that are capable of improving the efficiency of numerical implementation of the proposed MMC-based approach and at the same time preserving the complexity of structural topology, are introduced in Section 4. In Section 5, several representative examples are presented to illustrate the effectiveness of the proposed approach. Finally, some concluding remarks are provided in Section 6.

2. Problem formulation

In the MMC-based topology optimization approach, the material distribution of a

structure can be described by a so-called topology description functions (TDF) in the following form:

$$\begin{cases} \phi^s(\mathbf{x}) > 0, \text{ if } \mathbf{x} \in \Omega^s, \\ \phi^s(\mathbf{x}) = 0, \text{ if } \mathbf{x} \in \partial\Omega^s, \\ \phi^s(\mathbf{x}) < 0, \text{ if } \mathbf{x} \in D \setminus (\Omega^s \cup \partial\Omega^s), \end{cases} \quad (2.1)$$

where D represents a prescribed design domain and $\Omega^s \subset D$ denotes a region comprised by n components made of solid material. As shown in Guo et al. (2014), the TDF of the whole structure can be constructed as $\phi^s(\mathbf{x}) = \max(\phi_1(\mathbf{x}), \dots, \phi_n(\mathbf{x}))$ with $\phi_i(\mathbf{x})$ denoting the TDF of the i -th component (see Fig. 1 for a schematic illustration). In the present work, for two-dimensional (2D) case, as shown in Fig. 2, $\phi_i(\mathbf{x})$ is constructed as:

$$\phi_i(x, y) = 1 - \left(\frac{x'}{a_i}\right)^p - \left(\frac{y'}{b_i(x')}\right)^p, \quad (2.2)$$

with

$$\begin{Bmatrix} x' \\ y' \end{Bmatrix} = \begin{bmatrix} \cos \theta_i & \sin \theta_i \\ -\sin \theta_i & \cos \theta_i \end{bmatrix} \begin{Bmatrix} x - x_{0i} \\ y - y_{0i} \end{Bmatrix}, \quad (2.3)$$

and p is a relatively large even integer ($p = 6$ in this work). In Eq. (2.2) and Eq. (2.3), the symbols a_i , $b_i(x')$, (x_{0i}, y_{0i}) and θ_i denote the half-length, the variable half width, the coordinate of the center and the inclined angle (measured from the horizontal axis anti-clockwisely) of the i -th component (see in Fig. 2 for reference), respectively. It should be noted that the variation of the width of the component $b_i(x')$ can take different forms (Zhang et al. (2016c)), and in this work it is chosen as

$$b_i(x') = \frac{t_i^1 + t_i^2}{2} + \frac{t_i^2 - t_i^1}{2a_i} x', \quad (2.4)$$

where t_i^1 and t_i^2 are parameters used to describe the thicknesses of the component.

For 3D case, we use the following TDF to characterize the region occupied by the i -th component:

$$\phi_i(x, y, z) = 1 - \left(\frac{x'}{L_i^1}\right)^p - \left(\frac{y'}{g_i(x')}\right)^p - \left(\frac{z'}{f_i(x', y')}\right)^p, \quad (2.5)$$

with

$$\begin{Bmatrix} x' \\ y' \\ z' \end{Bmatrix} = \begin{bmatrix} R_{11} & R_{12} & R_{13} \\ R_{21} & R_{22} & R_{23} \\ R_{31} & R_{32} & R_{33} \end{bmatrix} \begin{Bmatrix} x - x_{0i} \\ y - y_{0i} \\ z - z_{0i} \end{Bmatrix}, \quad (2.6)$$

and

$$\begin{bmatrix} R_{11} & R_{12} & R_{13} \\ R_{21} & R_{22} & R_{23} \\ R_{31} & R_{32} & R_{33} \end{bmatrix} = \begin{bmatrix} c_b \cdot c_t & -c_b \cdot s_t & s_b \\ s_a \cdot s_b \cdot c_t + c_a \cdot s_t & -s_a \cdot s_b \cdot s_t + c_a \cdot c_t & -s_a \cdot c_b \\ -c_a \cdot s_b \cdot c_t + s_a \cdot s_t & c_a \cdot s_b \cdot s_t + s_a \cdot c_t & c_a \cdot c_b \end{bmatrix}, \quad (2.7)$$

respectively. In Eq. (2.7), $s_a = \sin \alpha$, $s_b = \sin \beta$, $s_t = \sin \theta$, $c_a = \sqrt{1 - s_a^2}$, $c_b = \sqrt{1 - s_b^2}$ and $c_t = \sqrt{1 - s_t^2}$ with α, β and θ denoting the rotation angles of the component from a global coordinate system $Oxyz$ to the local coordinate system $O'x'y'z'$ respectively (see Fig. 3 for reference). The central coordinate and the half-length of the component are represented by the coordinate (x_{0i}, y_{0i}, z_{0i}) and L_i^1 , respectively. Furthermore, the functions $g_i(x')$ and $f_i(x', y')$ in Eq. (2.5) are used to describe the thickness profiles of the component in y and z directions, respectively. In this work, $g_i(x')$ and $f_i(x', y')$ are simply chosen as

$$g_i(x') = L_i^2, \quad f_i(x', y') = L_i^3, \quad (2.8)$$

as shown in Fig. 4. Other forms of $g_i(x')$ and $f_i(x', y')$ can be found in Zhang et al. (2017c).

With use of the above expressions, the region Ω_i^s occupied by the i -th component can be described as:

$$\begin{cases} \phi_i(\mathbf{x}) > 0, & \text{if } \mathbf{x} \in \Omega_i^s, \\ \phi_i(\mathbf{x}) = 0, & \text{if } \mathbf{x} \in \partial\Omega_i^s, \\ \phi_i(\mathbf{x}) < 0, & \text{if } \mathbf{x} \in D \setminus (\Omega_i^s \cup \partial\Omega_i^s). \end{cases} \quad (2.9)$$

It is also obvious that $\Omega^s = \bigcup_{i=1}^n \Omega_i^s$. At this position, it is worth noting that topology optimization can also be carried out in the MMC-based solution framework without introducing TDF. Actually, the TDF is only employed for the convenience of performing FEA under fixed mesh. We refer the readers to Zhang et al. (2017a, 2017b, 2018b) for the implementation of the MMC-based topology optimization approach without use of TDFs.

Based on the above description, it is obvious that the layout of a structure can be solely determined by $\mathbf{D} = \left((\mathbf{D}^1)^\top, \dots, (\mathbf{D}^i)^\top, \dots, (\mathbf{D}^n)^\top \right)^\top$, a vector of design variables. To be specific, for 2D case, we have $\mathbf{D}^i = (x_{0i}, y_{0i}, a_i, \mathbf{d}_i^\top, \theta_i)^\top$, which contains the design variables associated with the i -th component with \mathbf{d}_i denoting the vector of geometry parameters related to $b_i(x')$. In 3D case, \mathbf{D} can be constructed in a similar way.

Under the MMC-based solution framework, a typical topology optimization problem can be formulated as follows:

$$\text{Find } \mathbf{D} = \left((\mathbf{D}^1)^\top, \dots, (\mathbf{D}^i)^\top, \dots, (\mathbf{D}^n)^\top \right)^\top$$

$$\begin{aligned}
& \text{Minimize } I = I(\mathbf{D}) \\
& \text{S. t.} \\
& g_k(\mathbf{D}) \leq 0, k = 1, \dots, m, \\
& \mathbf{D} \subset \mathcal{U}_{\mathbf{D}},
\end{aligned} \tag{2.10}$$

where $I(\mathbf{D})$, g_k , $k = 1, \dots, m$ are the objective function/functional and constraint functions/functionals. In Eq. (2.10), $\mathcal{U}_{\mathbf{D}}$ is the admissible set that design variable vector \mathbf{D} belongs to.

In the present study, structures are designed to minimize the structural compliance under the volume constraint of available solid material. Under this circumstance, the corresponding problem formulation can be specified as:

$$\begin{aligned}
& \text{Find } \mathbf{D} = \left((\mathbf{D}^1)^\top, \dots, (\mathbf{D}^i)^\top, \dots, (\mathbf{D}^n)^\top \right)^\top, \mathbf{u}(\mathbf{x}) \in \mathbf{H}^1(\Omega^s) \\
& \text{Minimize } C = \int_{\mathbf{D}} H(\phi^s(\mathbf{x}; \mathbf{D})) \mathbf{f} \cdot \mathbf{u} \, dV + \int_{\Gamma_t} \mathbf{t} \cdot \mathbf{u} \, dS \\
& \text{S. t.} \\
& \int_{\mathbf{D}} H^q(\phi^s(\mathbf{x}; \mathbf{D})) \mathbb{E} : \boldsymbol{\varepsilon}(\mathbf{u}) : \boldsymbol{\varepsilon}(\mathbf{v}) \, dV = \int_{\mathbf{D}} H(\phi^s(\mathbf{x}; \mathbf{D})) \mathbf{f} \cdot \mathbf{v} \, dV \\
& \quad + \int_{\Gamma_t} \mathbf{t} \cdot \mathbf{v} \, dS, \quad \forall \mathbf{v} \in \mathcal{U}_{\text{ad}}, \\
& \int_{\mathbf{D}} H(\phi^s(\mathbf{x}; \mathbf{D})) \, dV \leq \bar{V}, \\
& \mathbf{D} \subset \mathcal{U}_{\mathbf{D}}, \\
& \mathbf{u} = \bar{\mathbf{u}}, \text{ on } \Gamma_u,
\end{aligned} \tag{2.11}$$

where \mathbf{D} , \mathbf{f} , \mathbf{t} , \mathbf{u} , $\boldsymbol{\varepsilon} = \text{sym}(\nabla \mathbf{u})$ and $\bar{\mathbf{u}}$ are the design domain, the body force density, the prescribed surface traction on Neumann boundary Γ_t , the displacement field, the linear strain tensor and the prescribed displacement on Dirichlet boundary Γ_u , respectively. The symbol $H = H(x)$ denotes the Heaviside function with $H = 1$ if $x > 0$ and $H = 0$ otherwise. In Eq. (2.11), $\phi^s(\mathbf{x}; \mathbf{D})$ is the TDF of the whole structure while $q > 1$ is a penalization factor (in the present work, $q = 2$ is used). In Eq. (2.11), $\mathbb{E} = E^s / (1 + \nu) [\mathbb{I} + \nu^s / (1 - 2\nu^s) \boldsymbol{\delta} \otimes \boldsymbol{\delta}]$ is the fourth order elasticity tensor of the isotropic solid material with E^s , ν^s , \mathbb{I} and $\boldsymbol{\delta}$ denoting the Young's modulus as well as the Poisson's ratio of the solid material, symmetric part of the fourth order identity tensor and the second order identity tensor, respectively. The symbol $\mathcal{U}_{\text{ad}} = \{\mathbf{v} | \mathbf{v} \in$

$H^1(\Omega^s), \mathbf{v} = \mathbf{0} \text{ on } S_u\}$ represents the admissible set of virtual displacement vector \mathbf{v} and \bar{V} is the upper limit of the volume of the available solid material.

3. Solution strategies for multi-resolution topology optimization under the MMC-based framework

In this work, the super-element technique proposed by Nguyen et al. (2009) is adopted in the MMC-based solution framework to construct highly efficient multi-resolution topology optimization approach. As described in Nguyen et al. (2009), the basic idea of the super-element-based approach is that two sets of meshes with different resolutions are used for solving a topology optimization problem (see Fig. 5 for reference). The coarse mesh is used for interpolating the displacement field while the refined background mesh is used for describing the structural geometry with high resolution. This method has been proven to be very effective to reduce the computational cost associated with FEA in SIMP method. However, since the structural topology is still described by binary pixels/voxels, the number of design variables is still very large when large-scale multi-resolution topology optimization problems are considered. Besides, additional strategies (e.g., the density filtering) have to be introduced to eliminate numerical instabilities such as checkerboard pattern. Such treatments, however, will inevitably lead to boundary diffusion effect and the loss of structural details with small feature sizes. As a result, although the resolution of the density field is enhanced, the filtered structural boundary is still blurry, *and most important of all, the complexity of structural topology cannot be preserved in optimized structures*. This is due to the fact that in order to eliminate the checkerboard pattern, the filter radius should be greater than the size of coarse elements for FEA (not the size of the background mesh for topology representation!) and all structural features with characteristic sizes smaller than the filter radius (and the size of the FE mesh) will be erased out by the filtering operation.

However, if the super-element technique is applied under the MMC-based solution framework, the situation is totally different. This is because in the MMC approach, the structural geometry is described by a set of explicit geometrical parameters. This means that the structural topology has an *infinitely high resolution*. Based on this consideration, in the present work, we propose to combine both the advantages of the super-element approach and the MMC-based solution framework to tackle the multi-resolution topology optimization problems in a computationally efficient way.

In the present work, as the same in traditional treatments, we also intend to use a fixed FE mesh and an ersatz material model for FEA for simplicity, although adaptive FE mesh can also be applied to calculate structural responses since we have the explicit boundary representation in the MMC approach. Under this circumstance, a refined background mesh is also needed to identify the small structural features. It is, however, worth noting that, as can be seen clearly from the following discussions, unlike the traditional implicit topology optimization method, the refinement of the background mesh does not increase the number of design variables, and it only increases the computational effort associated with numerical integrations when the element stiffness matrix is formed.

With use of the super-element technique, the stiffness matrix of the i -th super-element can be calculated as (see Fig. 6 for a schematic illustration):

$$\mathbf{K}_i = \int_{\Omega_i} \mathbf{B}^\top \mathbf{D}_i(\mathbf{x}) \mathbf{B} d\Omega \approx \sum_{j=1}^{ng} E_{i,j} \mathbf{B}(\mathbf{x}_{i,j}^0)^\top \mathbf{D}_0 \mathbf{B}(\mathbf{x}_{i,j}^0) A_g, \quad (3.1)$$

where Ω_i represents the region occupied by the i -th super-element, $\mathbf{x} = (x, y)$ is the vector of spatial coordinates, \mathbf{B} and \mathbf{D}_i are the strain-displacement matrix and the constitutive matrix, respectively. In Eq. (3.1), ng represents the number of background elements in this super-element, \mathbf{D}_0 corresponds to the constitutive matrix of the solid material with unit Young's modulus and A_g is the area of a background element, respectively. $\mathbf{x}_{i,j}^0$ is the coordinate vector of the integration point (simply chosen as the central point of the corresponding background element in the present work) associated with the j -th background element in the i -th super-element. Numerical experiments show that this treatment is in general accurate enough. In addition, $E_{i,j}$ is the smeared Young's modulus of the j -th background element in the i -th super-element. Under the spirit of the ersatz material model, $E_{i,j}$ can be calculated through the corresponding nodal values of the TDF as

$$E_{i,j}(\phi^s) = \frac{E^s \left(\sum_{e=1}^4 \left(H(\phi_{i,j}^{se}) \right)^q \right)}{4}, \quad (3.2)$$

where $\phi_{i,j}^{se}$ is the value of TDF of the whole structure at the e -th node of element (i, j) , E^s is the Young's modulus of the solid material. $H = H(x)$ is the Heaviside function, which is often replaced by its regularized version $H_\epsilon(x)$ for numerical implementation. In the present work, $H_\epsilon(x)$ is taken as

$$H_\epsilon(x) = \begin{cases} 1, & \text{if } x > \epsilon, \\ \frac{3(1-\alpha)}{4} \left(\frac{x}{\epsilon} - \frac{x^3}{3\epsilon^3} \right) + \frac{1+\alpha}{2}, & \text{if } -\epsilon \leq x \leq \epsilon, \\ \alpha, & \text{otherwise,} \end{cases} \quad (3.3)$$

where ϵ and α are two small positive numbers used for controlling the length of the transition zone and avoiding the singularity of the global stiffness matrix, respectively.

Once the element stiffness matrix of each *super-element* is obtained, we can then assemble the global stiffness matrix \mathbf{K} , solve the displacement vector \mathbf{U} and obtain the structural compliance as $C = \mathbf{U}^\top \mathbf{K} \mathbf{U} = \sum_{i=1}^{NS} \mathbf{U}_i^\top \mathbf{K}_i \mathbf{U}_i$ with \mathbf{U}_i denoting the nodal displacement vector of the i -th super-element and NS representing the total number of super-elements. Then the sensitivity of the structural mean compliance with respect to a design variable d can be expressed as:

$$\begin{aligned} \frac{\partial C}{\partial d} &= - \sum_{i=1}^{NS} \mathbf{U}_i^\top \frac{\partial \mathbf{K}_i}{\partial d} \mathbf{U}_i \\ &= - \sum_{i=1}^{NS} \mathbf{U}_i^\top \left(\frac{E_0}{4} \sum_{j=1}^{ng} \left(\sum_{e=1}^4 q \left(H(\phi_{i,j}^{se}) \right)^{q-1} \frac{\partial H(\phi_{i,j}^{se})}{\partial d} \right) \mathbf{B}(\mathbf{x}_{i,j}^0)^\top \mathbf{D}_0 \mathbf{B}(\mathbf{x}_{i,j}^0) A_g \right) \mathbf{U}_i. \end{aligned} \quad (3.4)$$

For the volume constraint, we also have

$$\frac{\partial V}{\partial d} = \frac{1}{4} \sum_{j=1}^{NG} \sum_{e=1}^4 \frac{\partial H(\phi_j^{se})}{\partial d}. \quad (3.5)$$

In Eq. (3.4) and Eq. (3.5), the derivation of $\partial H(\phi_j^{se})/\partial d$ is trivial and will not be repeated here.

4. Numerical implementation aspects

In this section, we will discuss some numerical techniques that will be used to implement the proposed MMC-based multi-resolution topology optimization approach in a computationally efficient way. Actually, these techniques are not only applicable to the multi-resolution design case, but also capable of enhancing the computational efficiency of the original single-resolution oriented MMC approach (Guo et al. (2014), Zhang et al. (2016c)). Moreover, a so-called domain decomposition strategy is developed to increase the topological complexity of the optimized designs obtained by the proposed multi-

resolution topology optimization approach.

4.1 Generating the TDF and calculating sensitivities locally

As shown in Section 2, the geometry of a component is described by a p -th order hyperelliptic function. In our previous numerical implementations (e.g., Zhang et al. (2016c)), the TDF values associated with each component are calculated at every node of background FE mesh with use of Eq. (2.2)-Eq. (2.4) (for 2D case) or Eq. (2.5)-Eq. (2.8) (for 3D case). If, for example, a problem with 500 components and 1000×500 background elements is considered, the TDF nodal values must be calculated $(1000+1) \times (500+1) \times 500$ times to generate the TDF of the whole structure. This treatment will definitely consume a large amount of computational time and computer memory and is not suitable for solving large scale problems.

Actually, the nodal TDF values of the background FE mesh are used for the following three purposes: 1) describing the geometry of the components through Eq. (2.9); 2) calculating the Heaviside function used in the ersatz material model using Eq. (3.3) and 3) carrying out the sensitivity analysis as shown in Eq. (3.4)-Eq. (3.5). Actually, a component only occupies a small portion of the design domain, so it is not necessary to calculate the nodal values of TDF for the whole region. Furthermore, from Eq. (3.3), it can also be observed that both the Heaviside function and its derivative with respect to the TDF only vary in a narrow band $\Omega^{\text{BDY}} = \{\mathbf{x} | \mathbf{x} \in D, -\epsilon \leq \phi^s(\mathbf{x}) \leq \epsilon\}$ around the structural boundary and keep constant in rest regions. These insights inspire us that we can only generate and store the nodal values of the TDF of each component around its boundary *locally*. Since the size of an individual component is usually relative small compared with that of the whole design domain, this strategy can save the computational effort and memory to generate the corresponding TDF significantly.

In previous numerical implementation (e.g., Zhang et al. (2016c)), the formula $\phi^s = \max(\phi_1, \phi_2, \dots, \phi_n)$ is used to generate the TDF of whole structure. In the present work, the following well-known formula is used to approximate the max operation (Li and Fang (1997)):

$$\phi^s \approx \ln \left(\sum_{i=1}^n \exp(l\phi_i) \right) / l, \quad (4.1)$$

where l is a large positive number (e.g., $l = 100$). Using the same skill mentioned before, the exponent arithmetic in Eq. (4.1) can be carried out only around the boundary

region of each component. Numerical experiments indicate that this treatment can enhance the computational efficiency of generating the TDF of whole structure significantly as well.

In addition, since the Heaviside function's derivative with respect to the TDF only varies near the structural boundary, the sensitivities of the objective and constraint functions also can be calculated locally. It is worth noting that, although the sensitivity analysis in the MMC approach is not as straightforward as that in SIMP approach, the time cost for sensitivity analysis in the present work is, however, still much less than (or at least comparable to) that in the SIMP approach since the number of design variables is significantly reduced and there is no need to implement the chain rule differentiations resulting from the non-local filter operator. This point will be verified by the numerical examples provided in Section 5.

4.2 Domain decomposition strategy for preserving structural complexity

In this subsection, we shall discuss how to control the topological complexity in optimized designs. In the MMC approach, as shown in Fig. 7a, the components can move, morph, disappear, overlap and intersect with each other to constitute an optimized structure. Since the sensitivities are nonzero only in a narrow band near the structural boundary, and it is not difficult to observe that the sensitivities of the objective/constraint functions with respect to the design variables associated with a hidden component are zero. In other words, once a component is fully covered by others, it will remain unchanged in the following optimization process, unless the components cover it move away. Actually, this mechanism is responsible for the relatively simple topology of the optimized designs obtained by MMC approach, since many components may be covered by other components in the final design results (see Fig. 7a for reference).

Although a design with simple structural topology may be more favorable from manufacturing point of view, however, theoretical analysis indicated that optimal solutions of topology optimization problems may possess very complex structural topologies (e.g., the Michell truss (Sigmund et al. (2016), Dewhurst (2001))). As a result, it is very necessary to equip the MMC approach with the capability of producing optimized designs with complex structural topologies.

Actually, the aforementioned goal can be achieved by resorting to the so-called domain decomposition strategy. The key point is to restrain the range of the motions of

the components. As shown in Fig. 7b, in the proposed domain decomposition strategy, the design domain D is divided into several non-overlapped sub-regions $\Omega_i^{\text{sub}}, i = 1, \dots, ns$, where a specific number of components are distributed in them initially. During the entire process of optimization, it is required that the central point of every component initially located in a specific sub-region is always confined in that sub-region. This can be achieved easily by imposing some upper/lower bounds on the corresponding design variables of the involved components in the MMC-based problem formulation. In addition, this strategy actually does can provide a flexible way to control the structural complexity locally and adaptively. For example, if it is intended to produce an optimized structure with high structural complexity in a specific region $D_\alpha \subset D$, we can divide D_α into a relatively large number of sub-regions $\Omega_{j\alpha}^{\text{sub}}, j = 1, \dots, n_\alpha^s$ (i.e., $D_\alpha = \bigcup_{j=1}^{n_\alpha^s} \Omega_{j\alpha}^{\text{sub}}$) and put a relatively large number of components in each $\Omega_{j\alpha}^{\text{sub}}$. With use of this treatment, it can be expected that the corresponding optimized structure may have complex structural topology and structural features with length scales comparable with the characteristic sizes of the sub-regions in D_α . The effectiveness of this domain decomposition strategy will be verified numerically in the forthcoming section.

At this position, it is also interesting to note that if the sub-regions are selected as being coincided with the finite elements used for interpolating the displacement field, and one component is distributed in each sub-region (element) individually as shown in Fig. 8. Furthermore, if only the heights of the components are taken as design variables and the Young's modulus of each element is interpolated as $E_i = E^s(h_i/H_i)^p$ with h_i and H_i denoting the heights of the component and the corresponding finite element (sub-region) ($h_i \leq H_i$), respectively. Under the above treatment, it can be observed clearly that the proposed MMC-based multi-resolution topology optimization approach will reduce to the classical SIMP approach by defining h_i/H_i as the element density.

5. Numerical examples

In this section, two plane stress examples and one 3D example are investigated to illustrate the effectiveness of the proposed MMC-based method for multi-resolution topology optimization. The computational time and the optimized objective function values are compared with their counterparts obtained by efficient implementations of the SIMP method (i.e., 88-lines 2D code in Andreassen et al. (2010); 169-lines 3D code in Liu and Tovar (2014)). The MMA algorithm (Svanberg (1987)) is chosen as the optimizer

for both the MMC and the SIMP methods. Without loss of generality, all involved quantities are assumed to be dimensionless. The Young's modulus and the Poisson's ratio of the isotropic solid material are chosen as $E^s = 1$ and $\nu^s = 0.3$, respectively. In addition, all computations are carried out on a Dell-T5810 workstation with an Intel(R) Xeon(R) E5-1630 3.70GHz CPU, 128GB RAM of memory, Windows10 OS, and the computer code is developed in MATLAB 2016b. The values of parameters in Eq. (3.2) and Eq. (3.3) are taken as $q = 2$, $\epsilon = 2 \times \min(\Delta x, \Delta y, \Delta z)$ and $\alpha = 10^{-3}$, respectively, unless otherwise stated. Here $\Delta x, \Delta y$ and Δz are the sizes of the *background mesh* along three coordinate directions.

5.1 A cantilever beam example

In this example the well-known short cantilever beam problem is examined. The design domain, external load, and boundary conditions are all shown in Fig. 9. A 12×6 rectangular design domain is discretized by 1280×640 uniform background meshes for geometry representation. A unit vertical load is imposed on the middle point of right boundary of the design domain. The available volume of the solid material is $\bar{V} = 0.4V_D$ with V_D denoting the volume of the design domain. Fig. 10 shows the initial design composed of 576 components.

Firstly, the effectiveness of the domain decomposition strategy described in the previous section is tested. The design domain is divided into 1×1 , 6×3 , 12×6 sub-regions along the horizontal and vertical directions, respectively. For all cases, 1280×640 uniform bilinear plane stress elements with unit thickness are used for FEA. The corresponding optimized designs are shown in Fig. 11. It is obvious that as the number of sub-regions is increased, the optimal structural topology becomes more complicated, meanwhile the objective function value is slightly decreased. This reflects that the domain decomposition strategy is very effective to control the topological complexity of the optimized designs.

Next, the number of sub-regions is fixed as 12×6 and the efficiency of the proposed multi-resolution algorithm is investigated. As shown in Table 1, with respect to different resolutions of super-elements for FEA whilst keeping the same background mesh, the optimized designs, converged objective function values as well as the average time costs for some key parts of the corresponding optimization programs are compared. It is found that, as the number of the super-elements is gradually reduced, the time cost of the FEA

decreases rapidly. It should be noted that, for this example, the number of degree of freedom is 1642242 when the background mesh (with a number of 1280×640 elements) is used for structural analysis, while this number can be decreased to 26082 when 160×80 super-elements are used. Accordingly, as shown in Table 1, the average time cost of FEA is decreased sharply from 15.18s to 0.47s per optimization step.

As shown in Table 1, as the number of the super-elements gradually reduced (note that the number of sub-regions is fixed as 12×6), the corresponding value of the objective function is decreased as well. This can be explained by the fact that the stiffness of the structure will be overestimated when a coarser FE mesh is adopted. It can also be observed that the structural complexities of the five optimized structures are only slightly different with each other which indicates that the number of sub-regions is an important factor for determining the structural complexity of the final optimized structures. It can be imagined that more structural details can be introduced by dividing the design domain into more sub-regions. Furthermore, the corresponding values of the objective functions obtained by adopting the background meshes for FEA are also presented (the bold numbers in brackets in Table 1). One can find that, although the topologies of the optimized designs obtained under super-meshes with different resolutions are slightly different, the performances of the optimized structures are quite similar. This demonstrate clearly the effectiveness of the proposed multi-resolution approach in the sense that it can not only obtain appropriately optimized designs with much less time for FEA, but also control the structural complexity in a flexible way.

We also compared the result obtained using the proposed approach with that produced by the 88-line SIMP-based code presented by Andreassen et al. (2010), with $E_{\min} = 10^{-9}$, penalty factor $p = 3$ and the radius of density filter $r = 1.2$, respectively (see Table 2 for more details). By comparing the results shown in Table 1 and Table 2, it can be observed that: 1) The MMC method only needs relatively cheap time cost for updating the TDFs. 2) Most computational time in the SIMP approach is paid for FEA and design variable updating. For the same FE mesh, the computational time for FEA corresponding to the proposed method and the SIMP method are almost the same. If, however, the super-element technique is adopted, structural responses with enough accuracy can be obtained with much less computational time (about 1/30). Moreover, since the number of design variables in the MMC method is only 3456 (819200 in the SIMP approach), the computational efficiency for updating design variables by MMA

optimizer in the proposed approach can be improved by more than 200 times compared to that of the SIMP approach (actually 0.05s vs 14.70s!). As a result, when the same FE mesh is used, the average computational time for one optimization step is about 28.91s in the SIMP approach while the value of the same quantity is about 18.62s in the proposed approach, which can be further decreased to 3.13s when the super-element technique is employed. This comparison clearly verifies the efficiency of our method for solving large scale topology optimization problems. 3) Since no filter operation is applied to eliminate the numerical instabilities, the optimized designs obtained by the proposed approach are pure black-and-white and similar to the corresponding classical Michell truss, which is usually believed to be the theoretically optimal solution. This assertion can be further verified by comparing the value of the objective functional. Actually, by adopting the same interpolation strategy for Young's modulus of non-solid elements in SIMP approach, the value of the objective function for the optimized design obtained by 1280×640 FE meshes is 74.72, which is smaller than that (i.e., 80.29) of the design obtained by the SIMP approach.

5.2 The MBB example

The setting of this problem is described schematically in Fig. 12. A vertical load is imposed on the middle point of the top side with $f = 2$. For simplicity, only half of the design domain is discretized by 1280×640 uniform background meshes for geometry description. The upper bound of the volume of available solid material for this problem is set as $V = 0.4V_D$.

One half of the design domain is divided into 12×6 equal square sub-regions to preserve the structural complexity. The initial design of components is same as the first cantilever beam example (see Fig. 10 for reference). By discretizing the displacement field into 640×320 , 320×160 , 258×128 and 160×80 super-elements, as shown in Table 3, the computational time for FEA can be reduced by 25 times as compared with that associated with the case when the background mesh is adopted for FEA. Table 4 provides the optimization result obtained by the SIMP approach under a 1280×640 FE mesh with $E_{\min} = 10^{-9}$, penalty factor $p = 3$ and the radius of density filter $r = 1.2$, respectively. By comparing the corresponding results in Table 3 and Table 4, the same conclusions can be made as in the previous example.

5.3 A 3D box example

This example is actually an adaption of a similar example presented in Sigmund et al. (2016). For this example, as illustrated in Fig. 13a, the design domain is a $12 \times 10 \times 12$ 3D box, which is subjected to a pair of torque. The torque load is simulated by four concentrated point-forces as described in Fig. 13 and the magnitudes of these point forces are chosen as $f = 2$. The radii of the two red disks are 1.5 and their thicknesses are 0.15, respectively. Two void parts (the gray cylinder regions in Fig. 13a) are fixed as non-design domains. For simplicity, only 1/8 of the design domain is optimized. The admissible volume fraction of the solid material is 2%.

This problem is solved with use of the proposed approach for three sets of background meshes (i.e., $42 \times 35 \times 42$, $84 \times 70 \times 84$ and $126 \times 105 \times 126$, respectively). The same initial design containing 720 components, as shown in Fig. 13b, is adopted for all three tested cases. For comparison, this example is also solved by the SIMP method with use of its efficient numerical implementation described in Liu and Tovar (2014), with $E_{\min} = 10^{-9}$, penalty factor $p = 3$ and the radius of density filter $r = 1.5$, respectively. Optimality criterion (OC) method is used for updating the design variables of SIMP method. It should be pointed out that, current computer memory (128G) would be run out for FEA of $84 \times 70 \times 84$ traditional 8-node brick elements. So we used $42 \times 35 \times 42$ FE meshes for the SIMP approach, and $42 \times 35 \times 42$ super-elements for FEA of the proposed approach with respect to those three sets of background meshes, respectively.

The entire structure obtained by the SIMP method is shown in Fig. 14. The compliance of the 1/8 optimized structure is 120.49. Since the optimal solution obtained by the SIMP contains a lot of gray elements whose densities are neither zero nor one, we can only display the profile of the structure by using different values of the density threshold ρ_{th} . Actually, in our treatment, only the elements whose densities satisfy $\rho \geq \rho_{th}$ are plotted. Fig. 14a-Fig. 14c show the profiles of the optimized structure for $\rho_{th} = 0$, $\rho_{th} = 0.5$ and $\rho_{th} = 0.85$, respectively. It can be observed that the profiles are highly dependent on the value of ρ_{th} . And it is not an easy task to transfer the optimization result to CAD/CAE systems for further treatment (note that the structure may be disconnected when a large ρ_{th} is adopted while a small ρ_{th} may lead to infeasible design). Some post-processing techniques are necessary to extract the structural profile from the gray image.

The entire structures obtained by the proposed method under three sets of background

meshes are shown in Fig. 15a-Fig. 15c, respectively. It can be observed that the optimized design obtained with $42 \times 35 \times 42$ background meshes is an ellipsoid-like structure, which is quite different from the ball-like structure shown in Fig. 14a. This is due to the fact that since the minimum length scale in the optimized structures of MMC-based approach is limited by the characteristic size of the background mesh. Actually, for components with characteristic sizes less than the background mesh size, their contributions to structural stiffness cannot be detected by numerical integration procedure in FEA. Therefore, when the available material volume fraction is relatively small and the background mesh is not fine enough, it is extremely difficult to obtain a ball-like structure with very small thickness since the material distribution in MMC-based solution framework is purely black-and-white! Under this circumstance, only a lattice structure shown in Fig. 15a is selected to transmit the applied torque in an appropriate way. Actually, by using the same FEA strategy in SIMP method to reanalyze the 1/8 structure of Fig. 15a, the compliance value is 126.62, which is close to the result of SIMP approach. The ball-like structure, however, can be described in the SIMP-based solution framework since gray elements are allowed to exist in the final design. Furthermore, as shown in Fig. 15b and Fig. 15c, as the background mesh is refined, the corresponding optimized structure gradually changes to a ball-like structure with more material distributed around the applied forces and less material distributed elsewhere.

To more accurately measure the structural performances of the optimized designs with fine features of the MMC approach, we transferred the 1/8 structures of Fig. 15a-Fig. 15c to Abaqus directly (thanks again to the explicit nature of geometry description in the MMC-based approach) and perform the FEA with a set of $126 \times 105 \times 126$ meshes. It is found that the corresponding values of structural compliance are 297.97, 196.40 and 197.58 respectively, which reveals better designs can be obtained by increasing the resolution of background mesh. It is also worth noting that a direct comparison of the computational time between the proposed approach and the SIMP approach is not made for this example, since different optimizers are adopted for numerical optimization (i.e., OC method for the SIMP approach and MMA method for the proposed approach). However, since the number of design variables are only $720 \times 9 = 6480$ in the proposed approach and about 62000 in the SIMP-based approach, it can be expected that the computational time for numerical optimization associated with the MMC approach will be much less than that of the SIMP approach if the same optimizer is adopted.

6. Concluding remarks

In the present work, a highly efficient MMC-based approach for multi-resolution topology optimization is proposed. With use of this approach, both the numbers of the DOFs for finite element analysis and design variables for design optimization can be reduced substantially. Therefore, comparing with the traditional approaches, the corresponding computational time for the solution of large-scale topology optimization problems can be saved by about 1 order of magnitude. All these advantages can be attributed to the explicit nature of geometry description in the MMC-based solution framework. As a first attempt, only the minimum compliance design problems are considered in the present study to demonstrate the effectiveness of the proposed approach. It can be expected that the proposed approach can also find applications in other computationally intensive optimization problems (e.g., structural optimization considering geometry/material nonlinearity). Corresponding results will be reported elsewhere.

Acknowledgement

The financial supports from the National Key Research and Development Plan (2016YFB0201600, 2016YFB0201601, 2017YFB0202800, 2017YFB0202802), the National Natural Science Foundation (11402048, 11472065, 11732004, 11772026, 11772076), Program for Changjiang Scholars, Innovative Research Team in University (PCSIRT) and 111 Project (B14013) are gratefully acknowledged.

References

- Bendsøe MP, Kikuchi N (1988) Generating optimal topologies in structural design using a homogenization method. *Comput Methods Appl Mech Engrg* 71(2):197-224
- HyperWorks A (2013) OptiStruct-12.0 User's Guide. Altair Engineering Inc
- Simulia D (2011) Topology and Shape Optimization With Abaqus. Dassault Systemes Inc
- Aage N, Andreassen E, Lazarov BS, Sigmund O (2017) Giga-voxel computational morphogenesis for structural design. *Nature* 550(7674):84-86
- Borrvall T, Petersson J (2011) Large-scale topology optimization in 3D using parallel computing. *Comput Methods Appl Mech Engrg* 190:6201-6229
- Kim TS, Kim JE, Kim YY (2004) Parallelized structural topology optimization for eigenvalue problems. *Int J Solids Struct* 41(9-10):2623-2641
- Vemaganti K, Lawrence WE (2005) Parallel methods for optimality criteria-based topology optimization. *Comput Methods Appl Mech Engrg* 194:3637-3667
- Evgrafov A, Rupp CJ, Maute K, Dunn ML (2007) Large-scale parallel topology optimization using a dual-primal substructuring solver. *Struct Multidiscip Optim* 36(4):329-345
- Mahdavi A, Balaji R, Frecker M, Mockensturm EM (2006) Topology optimization of 2D continua for minimum compliance using parallel computing. *Struct Multidiscip Optim* 32(2):121-132
- Aage N, Poulsen TH, Gersborg-Hansen A, Sigmund O (2007) Topology optimization of large scale stokes flow problems. *Struct Multidiscip Optim* 35(2):175-180
- Aage N, Lazarov BS (2013) Parallel framework for topology optimization using the method of moving asymptotes. *Struct Multidiscip Optim* 47(4):493-505
- Wang S, Sturler ED, Paulino GH (2007) Large-scale topology optimization using preconditioned Krylov subspace methods with recycling. *Int J Numer Methods Engrg* 69(12):2441-2468
- Amir O, Bendsøe MP, Sigmund O (2009a) Approximate reanalysis in topology optimization. *Int J Numer Methods Engrg* 78(12):1474-1491
- Amir O, Stolpe M, Sigmund O (2009b) Efficient use of iterative solvers in nested topology optimization. *Struct Multidiscip Optim* 42(1):55-72
- Amir O, Sigmund O (2010) On reducing computational effort in topology optimization: how far can we go? *Struct Multidiscip Optim* 44(1):25-29
- Kim JE, Jang GW, Kim YY (2003) Adaptive multiscale wavelet-Galerkin analysis for

plane elasticity problems and its applications to multiscale topology design optimization. *Int J Solids Struct* 40(23):6473-6496

Stainko R (2005) An adaptive multilevel approach to the minimal compliance problem in topology optimization. *Commun Numer Meth En* 22(2):109-118

Guest JK, Smith Genut LC (2010) Reducing dimensionality in topology optimization using adaptive design variable fields. *Int J Numer Methods Engrg* 81(8):1019-1045

Yoon GH (2010) Structural topology optimization for frequency response problem using model reduction schemes. *Comput Methods Appl Mech Engrg* 199:1744-1763

Nguyen TH, Paulino GH, Song J, Le CH (2009) A computational paradigm for multiresolution topology optimization (MTOP). *Struct Multidiscip Optim* 41(4):525-539

Nguyen TH, Paulino GH, Song J, Le CH (2012) Improving multiresolution topology optimization via multiple discretizations. *Int J Numer Methods Engrg* 92(6):507-530

Guo X, Zhang WS, Zhong W (2014) Doing topology optimization explicitly and geometrically-a new moving morphable components based framework. *ASME J Appl Mech* 81(8):081009

Zhang WS, Li D, Zhang J, Guo X (2016a) Minimum length scale control in structural topology optimization based on the Moving Morphable Components (MMC) approach. *Comput Methods Appl Mech Engrg* 311:327-355

Guo X, Zhou JH, Zhang WS, Du ZL, Liu C, Liu Y (2017) Self-supporting structure design in additive manufacturing through explicit topology optimization. *Comput Methods Appl Mech Engrg* 323:27-63

Deng J, Chen W (2016) Design for structural flexibility using connected morphable components based topology optimization. *Sci China Technol Sc* 59(6):839-851.

Guo X, Zhang WS, Zhang J, Yuan J (2016) Explicit structural topology optimization based on moving morphable components (MMC) with curved skeletons. *Comput Methods Appl Mech Engrg* 310:711-748

Zhang WS, Zhang J, Guo X (2016b) Lagrangian description based topology optimization-a revival of shape optimization. *ASME J Appl Mech* 83(4):041010

Zhang WS, Yuan J, Zhang J, Guo X (2016c) A new topology optimization approach based on Moving Morphable Components (MMC) and the ersatz material model. *Struct Multidiscip Optim* 53(6):1243-1260

Zhang WS, Yang WY, Zhou JH, Li D, Guo X (2017a) Structural topology optimization through explicit boundary evolution. *ASME J Appl Mech* 84(1):011011

Zhang WS, Chen JS, Zhu XF, Zhou JH, Xue DC, Lei X, Guo X (2017b) Explicit three dimensional topology optimization via Moving Morphable Void (MMV) approach. *Comput Methods Appl Mech Engrg* 322:590-614

Zhang WS, Li D, Yuan J, Song JF, Guo X (2017c) A new three-dimensional topology optimization method based on moving morphable components (MMCs). *Comput Mech* 59(4):647-665

Zhang WS, Song JF, Zhou JH, Du ZL, Zhu YC, Sun Z, Guo X (2018a) Topology optimization with multiple materials via moving morphable component (MMC) method. *Int J Numer Methods Engrg* 113(11):1653-1675

Zhang WS, Li D, Zhou JH, Du ZL, Li BJ, Guo X (2018b) A Moving Morphable Void (MMV)-based explicit approach for topology optimization considering stress constraints. *Comput Methods Appl Mech Engrg* 334:381-413

Liu C, Du ZL, Zhang WS, Zhu YC, Guo X (2017) Additive manufacturing-oriented design of graded lattice structures through explicit topology optimization. *ASME J Appl Mech* 84(8):081008

Xue RY, Li R, Du ZL, Zhang WS, Zhu YC, Sun Z, Guo X (2017) Kirigami pattern design of mechanically driven formation of complex 3D structures through topology optimization. *Extreme Mech Lett* 15:139-144

Norato JA, Bell EK, Tortorelli DA (2015) A geometry projection method for continuum-based topology optimization with discrete elements. *Comput Methods Appl Mech Engrg* 293:306-327

Zhang SL, Norato JA, Gain AL (2016) A geometry projection method for the topology optimization of plate structures. *Struct Multidiscip Optim* 54(5):1173-1190

Zhang SL, Gain AL, Norato JA (2017d) Stress-based topology optimization with discrete geometric components. *Comput Methods Appl Mech Engrg* 325:1-21

Zhang SL, Gain AL, Norato JA (2018) A geometry projection method for the topology optimization of curved plate structures with placement bounds. *Internat J Numer Methods Engrg* 114(2):128-146

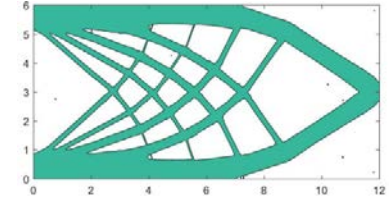
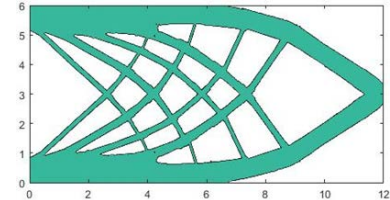
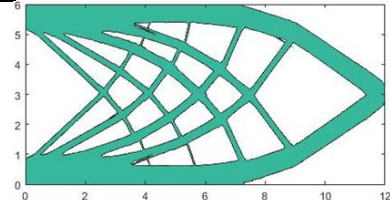
Zhang SL, Norato JA (2017) Optimal design of panel reinforcements with ribs made of plates. *ASME J Mech Des* 139(8):081403.

Zhang WH, Zhou Y, Zhou JH (2017e) A comprehensive study of feature definitions with solids and voids for topology optimization. *Comput Methods Appl Mech Engrg* 325:289-313

- Zhang WH, Zhao LY, Gao T (2017f) CBS-based topology optimization including design-dependent body loads. *Comput Methods Appl Mech Engrg* 322:1-22
- Hoang VN, Jang JW (2017) Topology optimization using moving morphable bars for versatile thickness control. *Comput Methods Appl Mech Engrg* 317:153-173
- Hou WB, Gai YD, Zhu XF, Wang X, Zhao C, Xu LK, Jiang K, Hu P (2017) Explicit isogeometric topology optimization using moving morphable components. *Comput Methods Appl Mech Engrg* 326:694-712
- Takaloozadeh M, Yoon GH (2017) Implementation of topological derivative in the moving morphable components approach. *Finite Elem Anal Des* 134:16-26
- Sun JL, Tian Q, Hu HY (2018) Topology optimization of a three-dimensional flexible multibody system via moving morphable components. *ASME J Comput Nonlinear Dyn* 13(2):021010
- Li XS, Fang SC (1997) On the entropic regularization method for solving min-max problems with applications. *Math Method Oper Res* 46(1):119-130
- Sigmund O, Aage N, Andreassen E (2016) On the (non-)optimality of Michell structures. *Struct Multidiscip Optim* 54(2):361-373
- Dewhurst P (2001) Analytical solutions and numerical procedures for minimum-weight Michell structures. *J Mech Phys Solids* 49(3):445-467
- Andreassen E, Clausen A, Schevenels M, Lazarov BS, Sigmund O (2010) Efficient topology optimization in MATLAB using 88 lines of code. *Struct Multidiscip Optim* 43(1):1-16
- Liu K, Tovar A (2014) An efficient 3D topology optimization code written in Matlab. *Struct Multidiscip Optim* 50(6):1175-1196
- Svanberg K (1987) The method of moving asymptotes-a new method for structural optimization. *Int J Numer Methods Engng* 24(2):359-373

Tables

Table. 1 Optimization results of the cantilever beam example obtained by the proposed approach with different FE meshes.

Optimized structure \ Performances	Compliance value	Number of FE mesh	Average time for constructing TDF per step (s)	Average time for FEA per step (s)	Average time for sensitivity analysis per step (s)	Average time for MMA per step (s)	Average time for one optimization step (s)
	73.60	1280×640	1.47	15.18	0.15	0.06	18.62
	73.61 (73.99)	640×320	1.19	6.54	0.12	0.05	9.69
	72.76 (73.84)	320×160	1.28	1.61	0.13	0.05	4.78

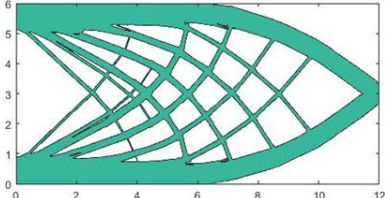
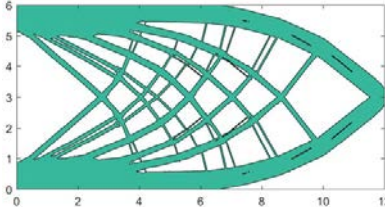
	<p>72.16 (73.70)</p>	<p>256×128</p>	<p>1.25</p>	<p>1.25</p>	<p>0.13</p>	<p>0.05</p>	<p>4.29</p>
	<p>71.30 (73.73)</p>	<p>160×80</p>	<p>0.81</p>	<p>0.47</p>	<p>0.10</p>	<p>0.03</p>	<p>3.13</p>

Table. 2 Optimization results of the cantilever beam example obtained with the SIMP approach.

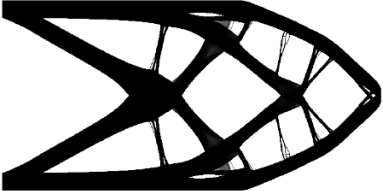
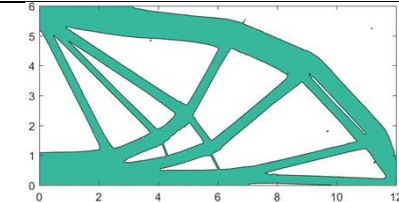
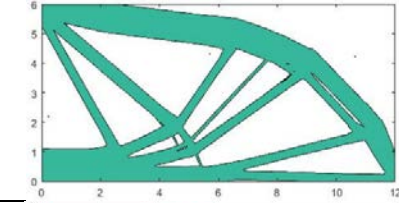
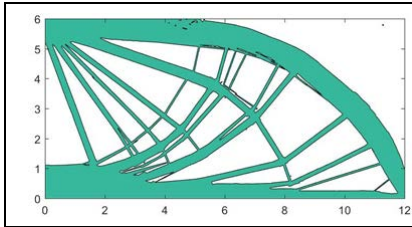
<div>Performances</div> <div>Optimized structure</div>	Compliance value	Number of FE mesh	Average time for FEA per step (s)	Average time for sensitivity analysis and filtering per step (s)	Average time for MMA per step (s)	Average time for one optimization step (s)
	80.29	1280×640	13.67	0.19	14.70	28.91

Table. 3 Optimization results of the MBB example obtained with the proposed approach under different FE meshes.

Performance Optimized structure	Compliance value	Number of FE mesh	Average solution time of TDF per step (s)	Average time cost of FEA per step (s)	Average time cost of sensitivities per step (s)	Average time cost of MMA solver per step (s)	Average time cost for one optimization step (s)
	96.59	1280×640	1.67	14.79	0.18	0.05	18.34
	94.78 (96.70)	640×320	1.77	6.56	0.19	0.06	10.22
	91.43 (96.25)	320×160	1.88	1.60	0.19	0.07	5.38
	90.32 (96.98)	256×128	1.56	1.06	0.16	0.05	4.52



87.87
(97.86)

160×80

1.35


0.59

0.14

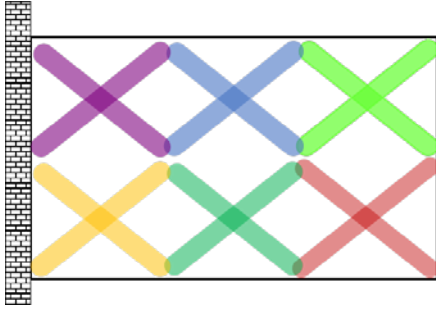
0.05

3.86

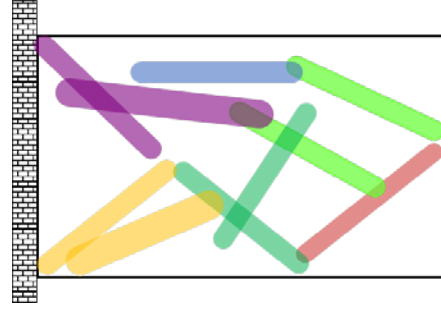
Table. 4 Optimization results of the cantilever beam example obtained with the SIMP approach.

Performance Optimized structure	Compliance value	Number of FE mesh	Average time cost of FEA per step (s)	Average time cost of sensitivities and filters per step (s)	Average time cost of MMA solver per step (s)	Average time cost for one optimization step (s)
	106.23	1280×640	11.78	0.20	12.51	24.80

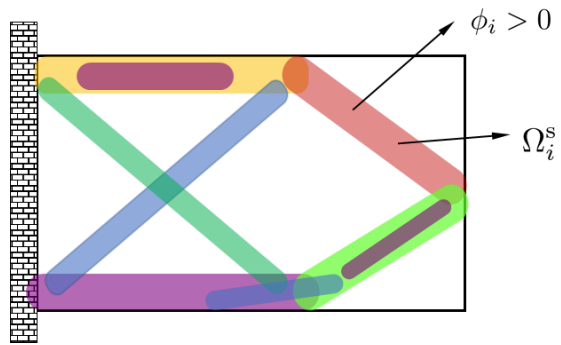
Figures



(a) The initial layout of the components.



(b) Optimization process.



(c) The optimized layout of the components.

Fig. 1 A schematic illustration of the MMC-based topology optimization method.

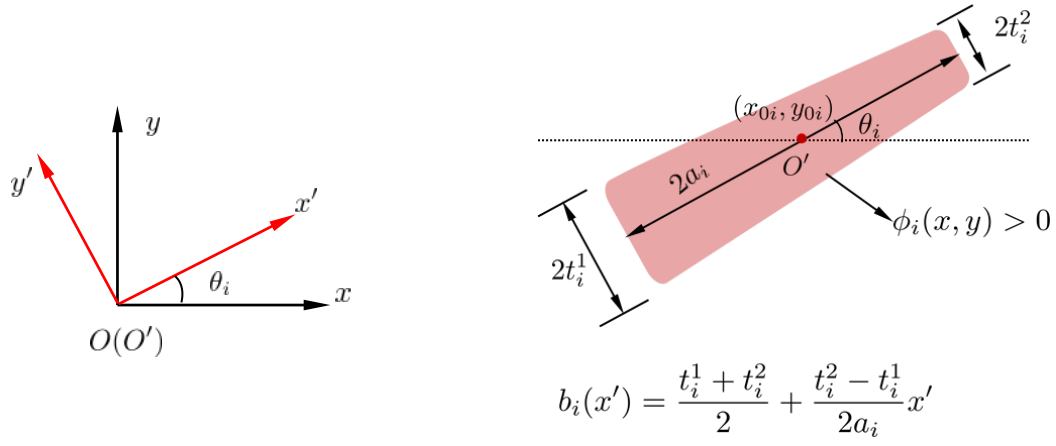


Fig. 2 The geometry description of a two-dimensional structural component.

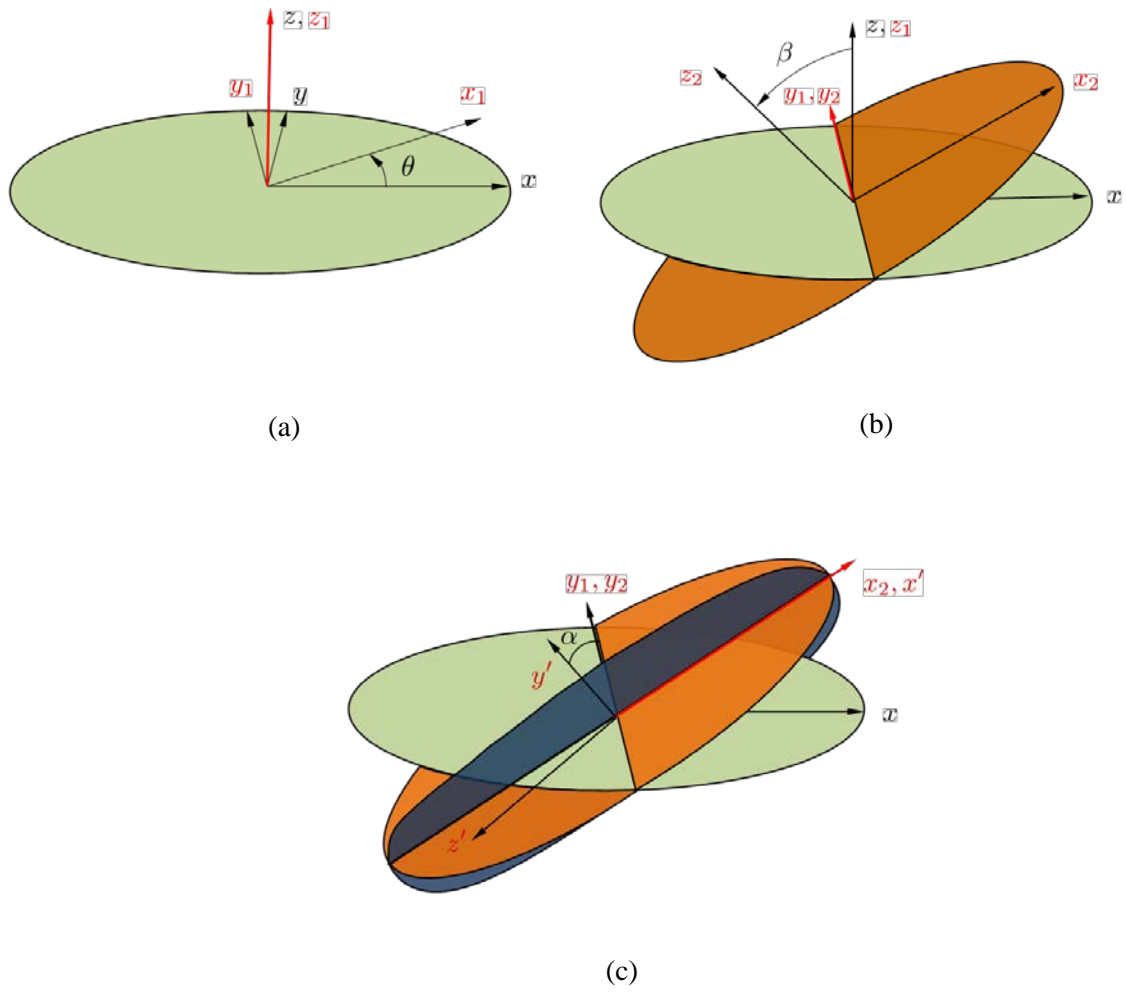


Fig. 3 Coordinate transformation associated with the three-dimensional components.

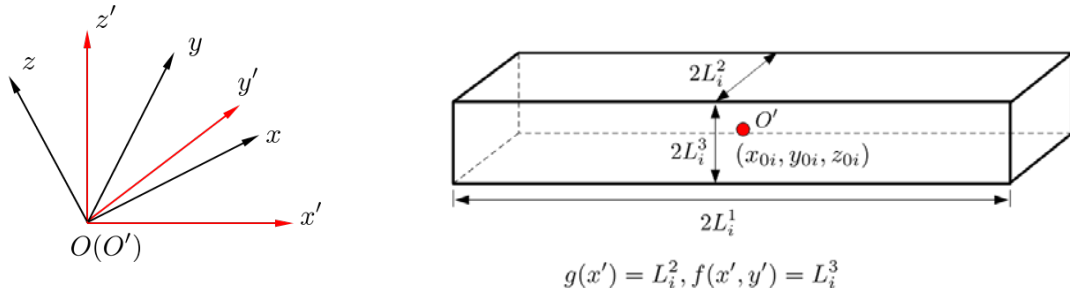


Fig. 4 The geometry description of a three-dimensional structural component.

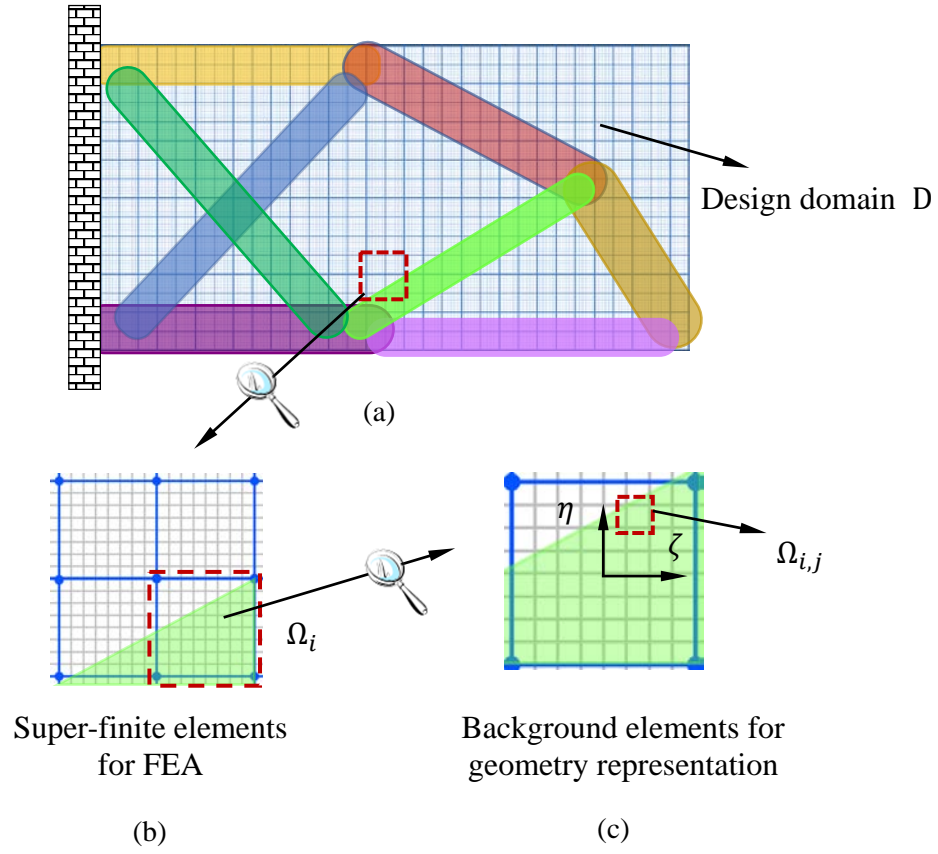


Fig. 5 A schematic illustration of the basic idea of the proposed MMC-based multi-resolution topology optimization.

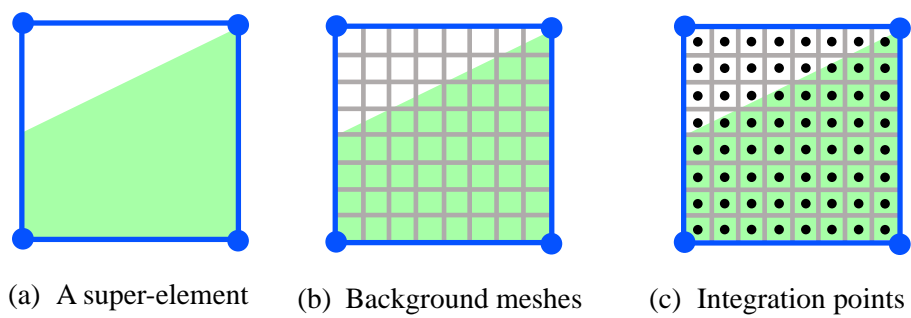
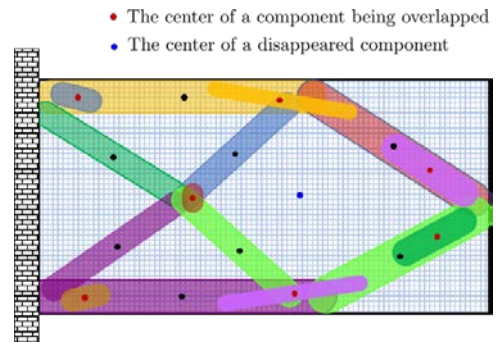
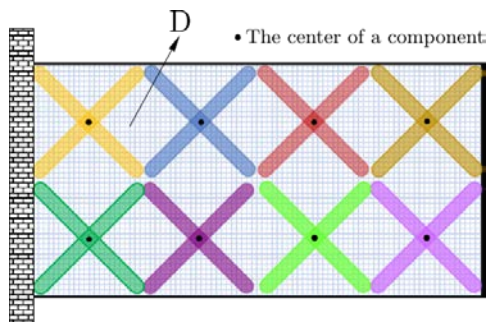
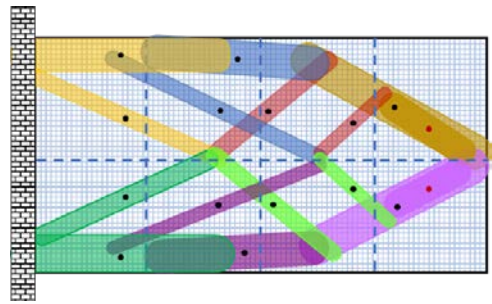
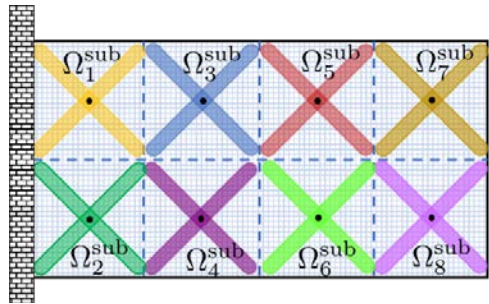


Fig. 6 A schematic illustration of a super-element, the background meshes and the integration points.



(a) MMC-based topology optimization without domain decomposition.



(b) MMC-based topology optimization with domain decomposition.

Fig.7 The basic idea of the domain decomposition strategy.

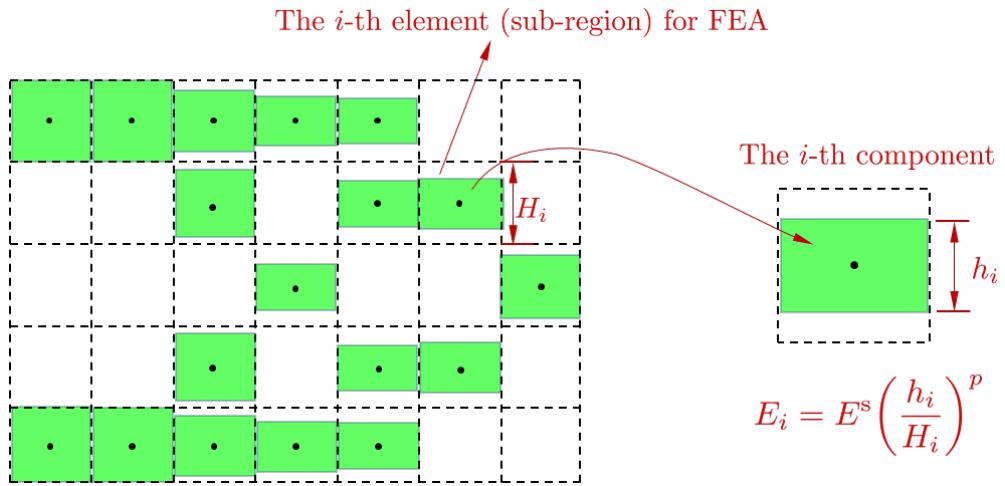


Fig.8 The degeneration of the MMC-based approach to the SIMP approach.

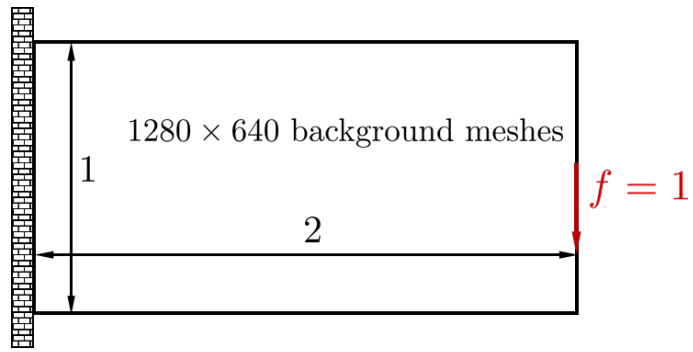


Fig. 9 The cantilever beam example.

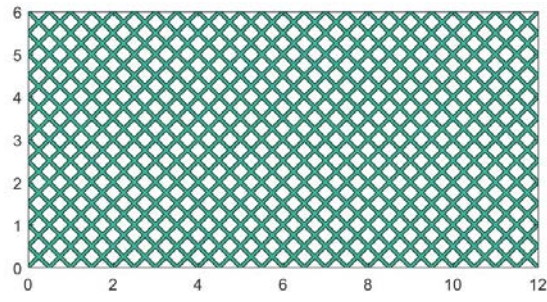
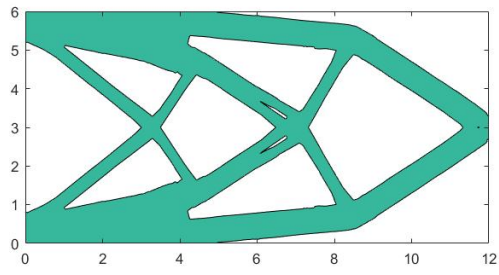
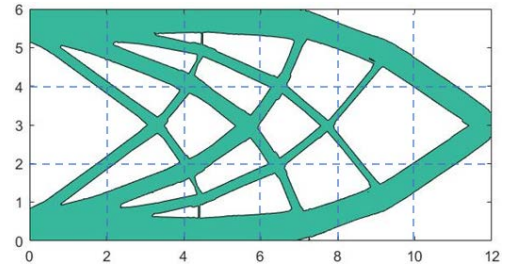


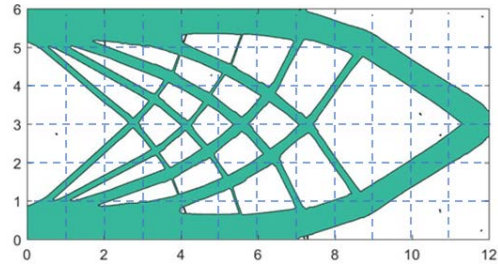
Fig. 10 The initial design of the cantilever beam example (576 components).



(a) Compliance value 74.63.

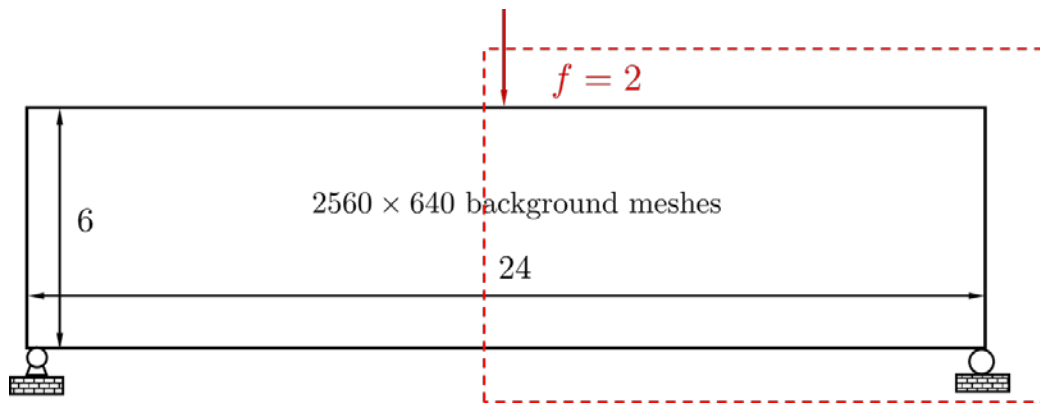


(b) Compliance value 73.60.

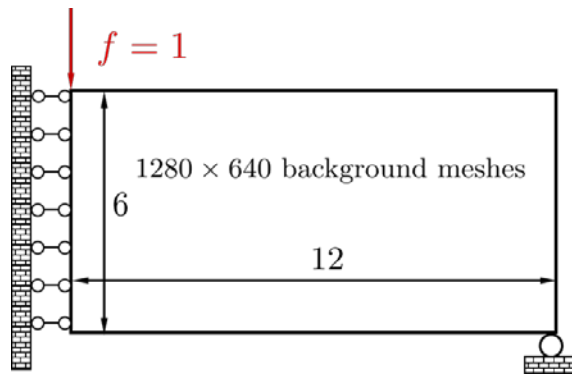


(c) Compliance value 73.59.

Fig. 11 The optimized structures obtained with domain decomposition strategy.

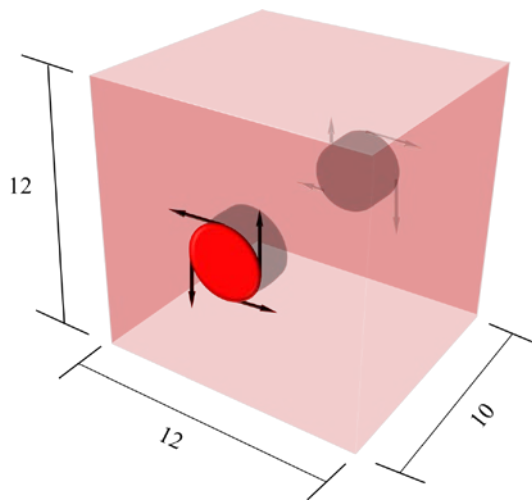


(a)

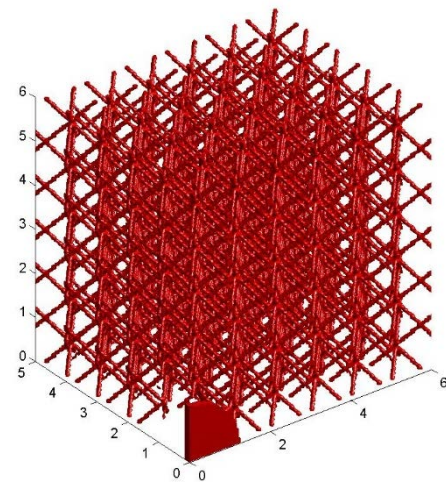


(b)

Fig. 12 The MBB example.



(a) The design domain.



(b) The initial design.

Fig. 13 The 3D box example.

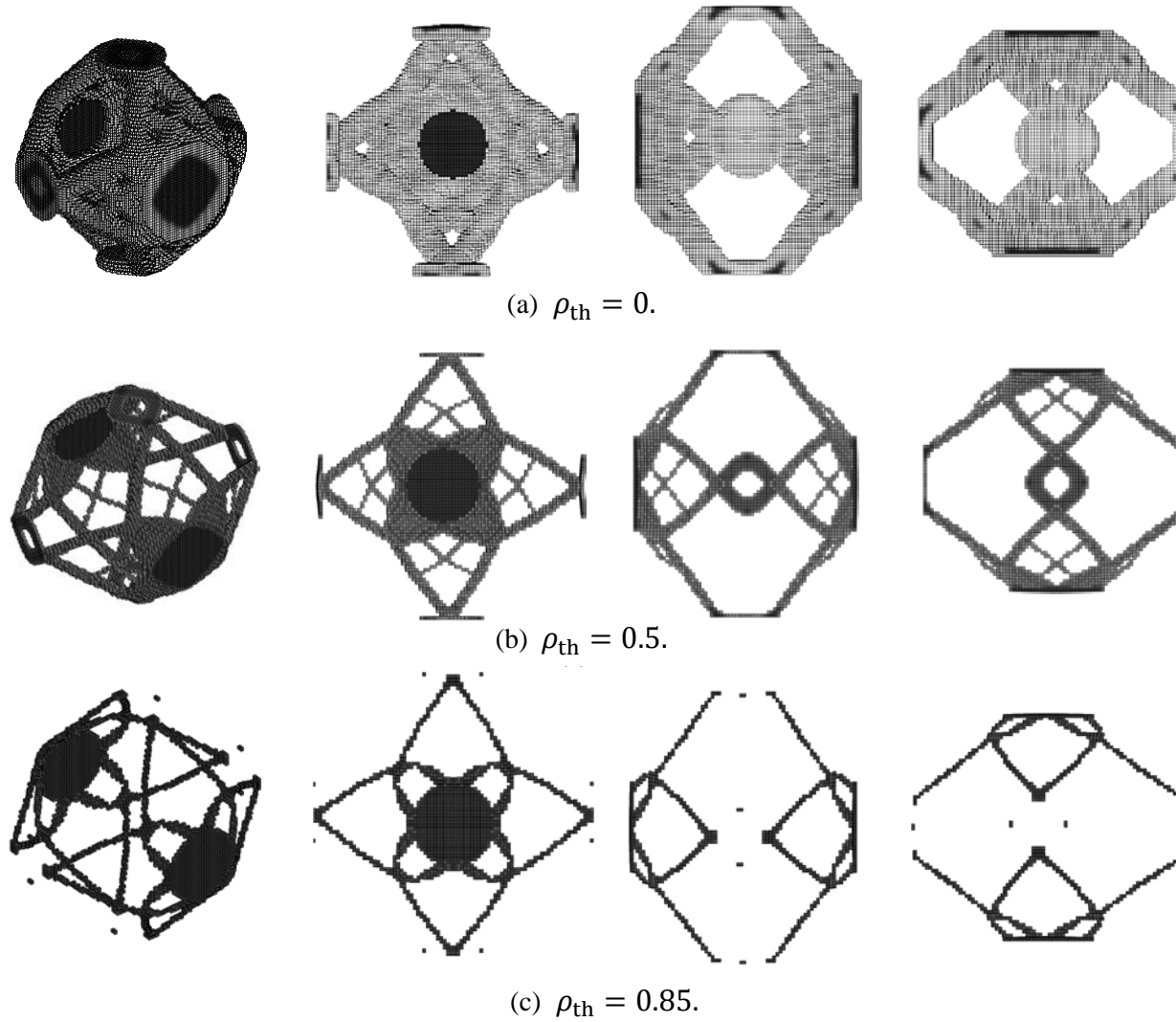


Fig. 14 The entire optimized structure of the 3D box example obtained with the SIMP method (displayed with different values of ρ_{th}).

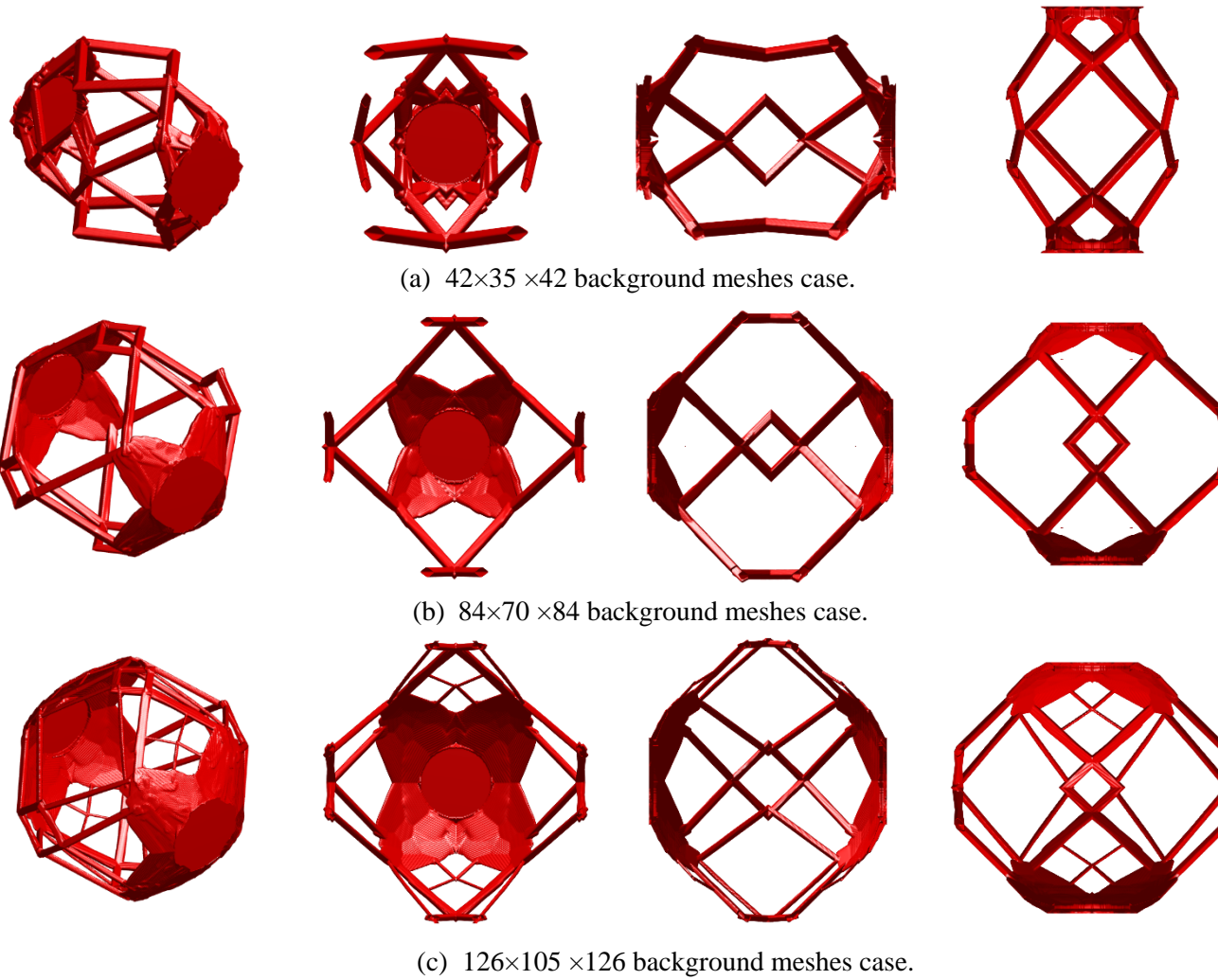


Fig. 15 The entire optimized structures of the 3D box example obtained with the proposed method.